Available online at www.sciencedirect.com
SCIENCE DIRECT®
International Journal of Solids and Structures 42 (2005) 2323–2344
INTERNATIONAL JOURNAL OF SOLIDS and STRUCTURES
www.elsevier.com/locate/ijsolstr

Enhancement of low velocity impact damage resistance of sandwich plates

Alexander P. Suvorov, George J. Dvorak *

Department of Mechanical, Aeronautical and Nuclear Engineering, Rensselaer Polytechnic Institute, 110 8th Street, Troy, NY 12180-3590, USA

Received 16 January 2004; received in revised form 16 September 2004
Available online 21 November 2004

Abstract

Conventionally designed sandwich plates used in marine and ship structures consist of thin, laminated composite face sheets bonded to a relatively thick, compressible structural foam core layer. In service, the external face sheet often makes low velocity contact with floating objects or moorings that may cause reversible local deflection of the face sheet and permanent compression or crushing of the underlying foam, resulting in interface delaminations. Extension of such interfacial cracks under service loads may impair structural integrity. Modified designs that protect the foam core by inserting a ductile interlayer under the external face sheet, first proposed in our recent paper [Dvorak, G.J., Suvorov, A.P., in press. Protection of sandwich plates from low velocity impact. Journal of Composite Materials 38], are analyzed here in much greater detail and compared with their conventional counterparts.

Two different interlayer materials are used, a stiff and incompressible polyurethane (PUR), and a compliant and compressible elastomeric foam (EF), together with the same face sheet and core materials. Response of the three different sandwich plate configurations of constant overall thickness is analyzed under uniformly applied load to a span of a continuous plate, and under forces imparted by two shapes of rigid indenters in a low velocity impact. The results show that the PUR interlayer reduces both overall and local deflections of the face sheet, and also the local compression of the foam core and the residual stresses left after unloading. The EF interlayer offers a much better protection against compression of the foam core, while magnifying both overall and local deflections. Both interlayers substantially reduce the strain energy release rates of interfacial cracks driven by residual stresses generated by foam core compression.

Keywords: Sandwich plates; Low velocity impact damage; Interfacial cracking

* Corresponding author. Tel.: +1 518 2766940; fax: +1 518 2762623.
E-mail address: dvorak@rpi.edu (G.J. Dvorak).

0020-7683/$ - see front matter © 2004 Elsevier Ltd. All rights reserved.
doi:10.1016/j.ijsolstr.2004.09.022

1. Introduction

Conventionally designed sandwich plates for marine structures typically consist of thin fibrous laminate face sheets bonded to a relatively thick layer of structural foam core. Vinyl ester matrices reinforced by glass or carbon fibers or fabrics, and PVC foam cores are the commonly used materials. Low velocity contact with floating objects or moorings can cause local deflection of the face sheet, permanent compression of the underlying foam, and nucleation of interfacial cracks. These may extend under service loads, possibly causing a catastrophic failure of the sandwich plate. Numerous experimental and theoretical studies have been conducted on this subject, for example, by Sun and Wu (1991), Lee et al. (1993), Wu et al. (1995), Zenkert (1995), Sun and Hasebe (2000), Lindholm and Abrahamsson (2003), Vadakke and Carlsson (2003), and others.

In a recent paper (Dvorak and Suvorov, in press), we have shown that the permanent compression of the foam core, followed by rebound of the face sheet upon unloading, gives rise to residual stresses that may drive an interfacial crack at some distance from the nucleation site. We then proposed a design modification of sandwich plates, involving use of ductile interlayers inserted between the face sheet and foam core. Under low velocity impact, the interlayer accommodates the face sheet deflection by fully reversible deformation. It also protects the foam core by reducing the extent of permanent compression and of the residual stress magnitude at the foam interface.

This approach to enhancement of damage resistance of sandwich plates is further explored in the present paper. A typical plate geometry is selected, with either a solid foam core, or an interlayer bonded between the external face sheet and a correspondingly thinner foam core layer. Two interlayer materials are considered for their effect on overall deflection of a single span of a continuous plate under uniformly distributed load, and on local response to low velocity impact: a relatively stiff and incompressible polyurethane (PUR), and a compliant and compressible elastomeric foam (EF); their properties, and those of the face sheet (F) and PVC foam core (C) are listed in Table 1.

The paper is organized as follows: Section 2 presents an elastic solution of the overall bending problem in both conventional and modified sandwich plates. Several quasi-static solutions of the low velocity impact problem for both plate designs are obtained in Section 3, together with the local dynamic response of the

Table 1
Dimensions and elastic properties of the sandwich plate constituents

Foam PVC H100	$E_c = 111\,\text{MPa}$, $\nu_c = 0.1$ Ductility 10–60%	$h_c + t_e = 50\,\text{mm}$
Polyurethane (PUR) Isoplast 101	E_e=1500 MPa, $\nu_e = 0.49$ Ductility 160%	$t_e = 5\,\text{mm}$
Elastomeric foam (EF)	$E_e = 10\,\text{MPa}$, $\nu_e = 0$ Ductility > 100%	$t_e = 5\,\text{mm}$
Face sheet $(0/\pm45/90)_s$ AS4/3501-6 Graphite/epoxy laminate	$E_1 = E_2 = 55022\,\text{MPa}$, $E_3 = 10792\,\text{MPa}$ $G_{12} = 21319\,\text{MPa}$, $G_{13} = G_{23} = 4953\,\text{MPa}$ $\nu_{12} = 0.29$, $\nu_{13} = \nu_{23} = 0.2487$ Ductility low	$t_f = 3.6\,\text{mm}$
Cylindrical indenter, Fig. 3		Radius $R_i = 25\,\text{mm}$
Flat indenter, Fig. 3		$d_i = 20\,\text{mm}$
Sandwich plate, Fig. 1		Height $h = 57.2\,\text{mm}$

plates to several impact velocities. Strain energy release rates for cracks extending along different interfaces are evaluated in Section 4.

2. Overall bending of the sandwich plate

Consider a single section of a continuous sandwich plate with periodically spaced supports. Fig. 1 shows schematically such sections, one of a conventional plate, and another of a plate with a ductile interlayer inserted between face sheet and foam core. Both plates have the same total thickness $h \ll L$ and the span length. Large plate width is assumed in the y-direction, implying a state of plane strain. The displacement boundary conditions for a section of a continuous plate are

$$\begin{aligned} &u(x=-L/2,z)=u(x=L/2,z)=0\\ &w_{,x}(x=-L/2,z)=w_{,x}(x=L/2,z)=0\\ &w(x=-L/2,-h/2)=w(x=L/2,-h/2)=0 \end{aligned} \tag{1}$$

where u, w are horizontal and vertical displacements, respectively. The traction boundary conditions are consistent with application of distributed load q, e.g., water pressure, which causes overall bending of the plate,

$$\begin{aligned} &\sigma_{zz}(x,h/2)=q(x), \quad \sigma_{xz}(x,h/2)=0\\ &\sigma_{zz}(x,-h/2)=0, \quad \sigma_{xz}(x,-h/2)=0 \end{aligned} \tag{2}$$

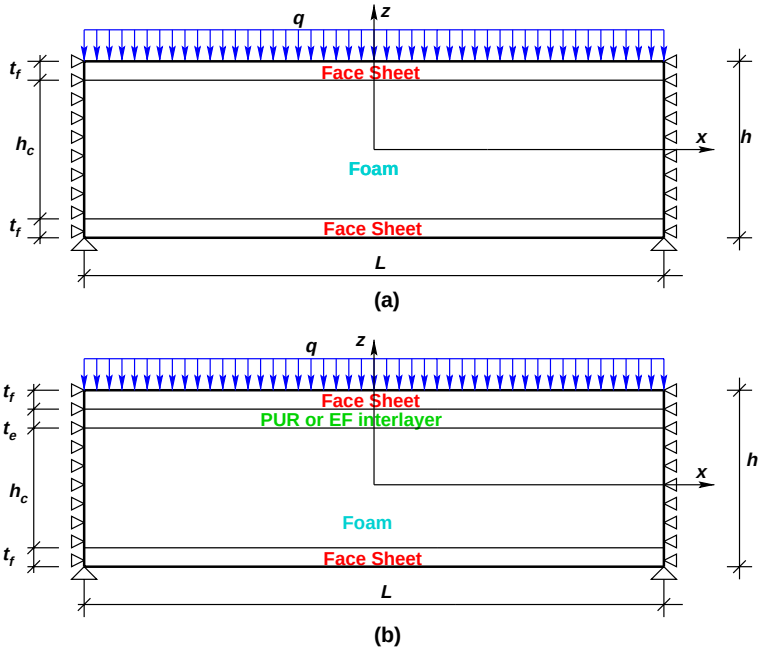

Fig. 1. Sandwich plate with or without an interlayer, subjected to a distributed load q.

In the overall bending analysis, each layer is regarded as a linear elastic solid. Orthotropic material symmetry is admitted in the face sheets, while the interlayer and foam core materials are assumed to be isotropic. The coefficients of the (6×6) stiffness matrix $\boldsymbol{L}$ for the general orthotropic material are given in Appendix A, in terms of engineering moduli: Young's moduli E_{ij}, shear moduli G_{ij} and Poisson's ratios ν_{ij}.

A finite element ABAQUS software (2001) was employed to evaluate deflections and stress distributions. The following traction boundary conditions were considered:

$$\begin{aligned} q &= q_0, \quad -L/2 \leqslant x \leqslant L/2 \\ q &= q_0 \cos\frac{\pi x}{2d}, \quad -d \leqslant x \leqslant d \end{aligned} \tag{3}$$

where $2d$ is a given length. Due to the symmetry of the problem with respect to $x = 0$, only half of the beam was discretized. The layer material properties are listed in Table 1. The face sheets were represented by quasi-isotropic, symmetric laminated plates. The properties of this laminated plate were found using homogenization method (Gudmundson and Zang, 1993) and derived from the properties of a single AS4/3501-6 graphite/epoxy ply given in Sun 1991. A PVC H100 foam was selected for the core material. The stiff interlayer properties are those of the polyurethane Isoplast 101 resin manufactured by Dow Plastics. The elastomeric foam moduli were selected as typical of the actual range for the closed cell polyethylene foam $E_e = 0.2$–30 MPa (Gibson and Ashby, 1997). Layer thicknesses and elastic moduli appear in Table 1.

Fig. 2 shows the bottom surface deflections w of sandwich plate configurations of Fig. 1, loaded by a uniformly distributed load $q = -0.1$ MPa. Results were obtained both for the conventionally designed plate without an interlayer (Fig. 1a) and for the modified design of Fig. 1b, with relatively stiff and compliant interlayers. The results indicate that the polyurethane (PUR) interlayer, which is much stiffer than the foam core, causes a small reduction of the overall deflection, while the very compliant and incompressible elastomeric foam (EF) interlayer magnifies the deflection substantially.

Tables 2 and 3 show the stresses found in the sandwich plate with interlayer (PUR or EF) or without interlayer (O) subjected to cosine type loading $(3)_2$ with $q_0 = -2$ MPa, $2d = 100$ mm, or uniform loading with $q = -0.1$ MPa. The stresses are evaluated at the centroids of the elements. The parameter ϵ is a small number equal to the half length along z-axis of the closest finite element.

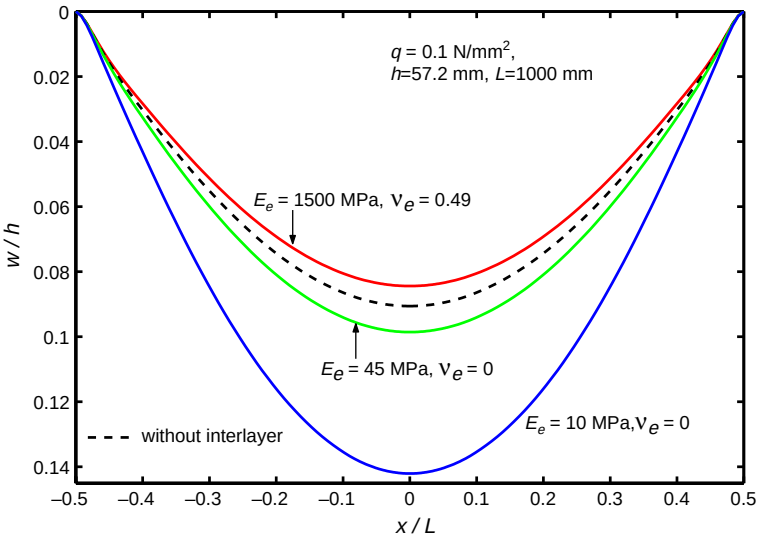

Fig. 2. Deflection of the bottom surface of sandwich plates subjected to distributed load $q = -0.1$ MPa; plate dimensions and material properties are listed in Table 1.

Table 2
Stresses in the sandwich plate subjected to $q(x) = -2\cos\frac{\pi x}{2d}$ on the top surface $z = h/2$, $d = 50\,\text{mm}$

	$\sigma_{xz}(x = -L/2 + L/10)$			$\sigma_x(x = 0)$			$\sigma_z(x = 0)$		
	PUR	EF	O	PUR	EF	O	PUR	EF	O
$z = h/2 - \epsilon$	−0.17	−0.24	−0.17	−126.1	−152.2	−133.2	−2	−2	−2
$z = h/2 - 0.5t_f$	−0.69	−0.76	−0.68	−60.3	−16.0	−53.8	−2	−2	−2
$z = h/2 - t_f + \epsilon$	−1.09	−0.98	−1.09	4.85	119.3	25.0	−1.91	−1.7	−1.89
$z = h/2 - t_f - t_e + \epsilon$	−1.2	−0.93	−1.15	4.94	−0.1	−0.032	−1.63	−1.52	−1.7

O—original design without interlayer; PUR, EF design with interlayers.

Table 3
Stresses in the sandwich plate subjected to uniform load $q(x) = -0.1\,\text{MPa}$ on the top surface $z = h/2$

	$\sigma_{xz}(x = -L/2 + L/10)$			$\sigma_x(x = 0)$			$\sigma_z(x = 0)$		
	PUR	EF	O	PUR	EF	O	PUR	EF	O
$z = h/2 - \epsilon$	−0.12	−0.19	−0.11	−21.7	−17.1	−21.7	−0.1	−0.1	−0.1
$z = h/2 - 0.5t_f$	−0.46	−0.58	−0.45	−17.8	−10.5	−17.6	−0.1	−0.1	−0.1
$z = h/2 - t_f + \epsilon$	−0.72	−0.71	−0.71	−14	−3.9	−13.5	−0.1	−0.1	−0.1
$z = h/2 - t_f - t_e + \epsilon$	−0.77	−0.65	−0.75	−0.15	−0.013	−0.028	−0.092	−0.092	−0.092

O—original design without interlayer; PUR, EF design with interlayers.

3. Low-velocity impact by a rigid indenter

3.1. Solution procedure

Local contact of the sandwich plate with a foreign object is simulated here by quasi-static loading applied to the top face sheet by cylindrical or flat rigid indenters. The plane strain deformation state of Section 2 is retained here. Analytic solutions of such problems are available for elastic layers on both rigid (Johnson, 1987) and elastic substrates (Barovich et al., 1964; Gupta et al., 1973). Since inelastic deformations of the core and interlayers are expected to have a significant effect on residual stress states and interface crack nucleation, a finite element solution with ABAQUS software (2001) was used in evaluation of results. The solution domain and boundary conditions appear in Fig. 3. Both indenter contours are shown, together with the different layups of the sandwich plates examined herein. According to the results of exploratory calculations, indentation of the face sheet caused by a given magnitude of applied force, and subsequent damage to the interfaces, reach a maximum when the indenter makes contact at one of the supports of the plate. Therefore, the bottom edge of the plate, at $z = -h/2$, $-l \leqslant x \leqslant l$, is supported here by a frictionless rigid half space. Symmetry of the loading and deformation about $x = 0$ is assumed in the absence of shear loads.

The displacement and traction boundary conditions then become,

$$\begin{aligned} &u(0,z) = 0, \quad w(x,-h/2) = 0, \qquad u, w \to 0 \ \text{ as } \ x \to \infty \\ &\sigma_{xz}(0,z) = \sigma_{xz}(x,-h/2) = 0, \quad \sigma_{zz}(x,h/2) = \sigma_{xz}(x,h/2) = 0 \qquad x > d \\ &\int_{-d}^{d} \sigma_{zz}(x,h/2)\,\mathrm{d}x = P, \quad \int_{-d}^{d} \sigma_{xz}(x,h/2)\,\mathrm{d}x = 0 \end{aligned} \tag{4}$$

where d (or d_i) is equal to one half of the contact width and P is the force applied to the indenter.

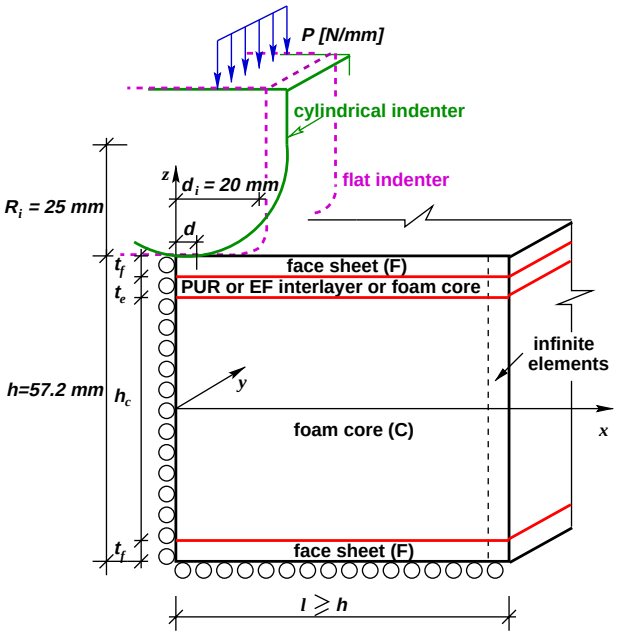

Fig. 3. Geometry of the sandwich plate impacted by a cylindrical or a flat indenter.

Elastic properties of the face sheets (F) in Table 1 are retained, but those of the interlayers and foam core are expanded beyond the elastic range. In particular, the structural foam core material (C) is assumed to be elastic in its initial response, up to its compression strength $\sigma_c^0 > 0$, and then undergo inelastic deformation at compressive stresses $|\sigma_c| > \sigma_c^0$, with the plastic strain ϵ_{pl} in uniaxial compression test related to the applied compressive stress σ_c by the power-law strain hardening equation,

$$\epsilon_{pl} = \left(\frac{|\sigma_c| - \sigma_c^0}{H}\right)^n, \quad |\sigma_c| \geqslant \sigma_c^0 \tag{5}$$

This constitutive relation was implemented in the crushable foam model provided by ABAQUS and described in Appendix B. The PVC H100 structural foam with Young's modulus $E_e = 111\,\text{MPa}$ was used in calculations. A low Poisson's ratio $v = 0.1$ was selected to improve convergence of the solution in the inelastic range. The parameters in (5) were set equal to $H = 2\,\text{MPa}$, $n = 2$. This choice of parameters, although not representing a horizontal plateau in stress–strain curve observed in experiments (Gibson and Ashby, 1997) provided good convergence of the solution and at the same time low hardening. The compression strength of the foam in hydrostatic compression was taken equal to that in uniaxial compression $\sigma_c^0 = 1.7$ MPa obtained by Lindholm and Abrahamsson (2003). The tensile strength was selected as $\sigma_t^0 = 0.1\sigma_c^0$ (ABAQUS 6.2 Standard User's Manual) and $\sigma_t^0 = 0.8\sigma_c^0$ for evaluation of energy release rates.

The polyurethane *Isoplast* 101 (PUR) interlayer was modeled as an incompressible Neo–Hookean material using hyperelastic material model of ABAQUS. The strain energy for a general Neo–Hookean material is given by (Blatz, 1971; Ogden, 1984),

$$W(\boldsymbol{F}) = \frac{\mu}{2}(\text{tr}\boldsymbol{C} - 3) + \left(K - \frac{2}{3}\mu\right)(\det \boldsymbol{F} - 1) - \left(K + \frac{\mu}{3}\right)\ln(\det \boldsymbol{F}) \tag{6}$$

where μ is the shear modulus, K is the bulk modulus, $\boldsymbol{F}$ is the deformation gradient tensor, and $\boldsymbol{C} = \boldsymbol{F}^{\mathrm{T}}\boldsymbol{F}$ is the right deformation tensor. The Green's deformation tensor taken on the reference configuration is found as $\boldsymbol{E} = \frac{1}{2}(\boldsymbol{C} - \boldsymbol{I})$. For an incompressible material, (6) can be simplified to

$$W(\boldsymbol{F}) = \frac{\mu}{2}(\mathrm{tr}\boldsymbol{C} - 3) \tag{7}$$

The eigenvalues of matrix $\boldsymbol{C}$ are denoted by $\lambda_1^2,\ \lambda_2^2,\ \lambda_3^2$; the λ_i are principal stretches. Then, the strain energy for incompressible Neo–Hookean material can be written as

$$W(\boldsymbol{F}) = \frac{\mu}{2}(\lambda_1^2 + \lambda_2^2 + \lambda_3^2 - 3) \tag{8}$$

The first Piola–Kirchhoff stress tensor can be found from (8) as

$$T_{ij} = \frac{\partial W}{\partial F_{ij}} \tag{9}$$

and the Cauchy stress is found as $\boldsymbol{\sigma} = (\det \boldsymbol{F})^{-1}\boldsymbol{T}\boldsymbol{F}^{\mathrm{T}}$. For an incompressible material, $\det \boldsymbol{F} = 1$.

3.2. Face sheet and foam core interface deflections

The magnitude of the applied force P per unit width of the plate in the y-direction was selected in the range of 0–200 N/mm for the cylindrical indenter and up to 300 N/mm for the flat indenter. These selections allowed inelastic deformation or crushing of the foam core, but kept the deflections and the membrane stresses in the face sheet within allowable strength limits. The results that follow show the effects of the two selected interlayer materials in reducing the magnitude of foam core deformation relative to that caused in conventionally designed sandwich plates.

Fig. 4a and b present a comparison of the indentations caused at the center of the contact zone in different sandwich plate designs by the cylindrical and flat indenters, loaded by P. As expected, deflection of the face sheet supported by the stiff and incompressible PUR interlayer is smaller than that of the face sheet in the conventionally designed plate. The plate with a compliant elastomeric foam (EF) interlayer experiences the largest surface deflection. Examination of the force-deflection diagrams reveals that both the conventionally designed and modified plate with the PUR interlayer exhibit deviations from linear response at $P \approx 100-150$ N/mm. This is associated with onset of crushing of the underlying foam core, which allows the face sheet deflections to increase at a higher rate with the applied force. In contrast, the deviation from linearity in the plate with the compliant but compressible EF interlayer starts at much higher applied force of $P \approx 160$–200 N/mm. This is not unexpected, as the EF interlayer is capable of accommodating large compressive deformations at relatively low compressive stresses. The load is thus carried mostly by the elastically responding face sheet, and onset of core crushing is deferred to higher load levels. Of course, as suggested by Figs. 2 and 4, the very compliant EF interlayer magnifies both overall deflection of the plate, and local deflection of the face sheet.

Fig. 5a and b show the deflection profiles of the interface of the foam core for the two indenters and loading conditions used in Fig. 4a and b. The cylindrical indenter causes much higher local deflections, and the PUR interlayer is seen to reduce their magnitude at the foam core surface. Both indenters appear to affect a relatively large area of the plate. Their effect is felt even at the distance of 60–70 mm from the center point of contact, where the deflection no longer depends on the shape of the indenter and amounts to a small fraction of the maximum deflection under the loaded indenter.

Of interest in design is the relative effect of the interlayer thickness and elastic modulus on the deflection of the foam core. This is presented in Fig. 6, which shows the magnitude of the maximum deflection (at $x = 0$ in Fig. 3), caused by the cylindrical indenter at the foam core interface with an incompressible interlayer. The selected ranges of elastic moduli and thicknesses of the interlayer should accommodate most

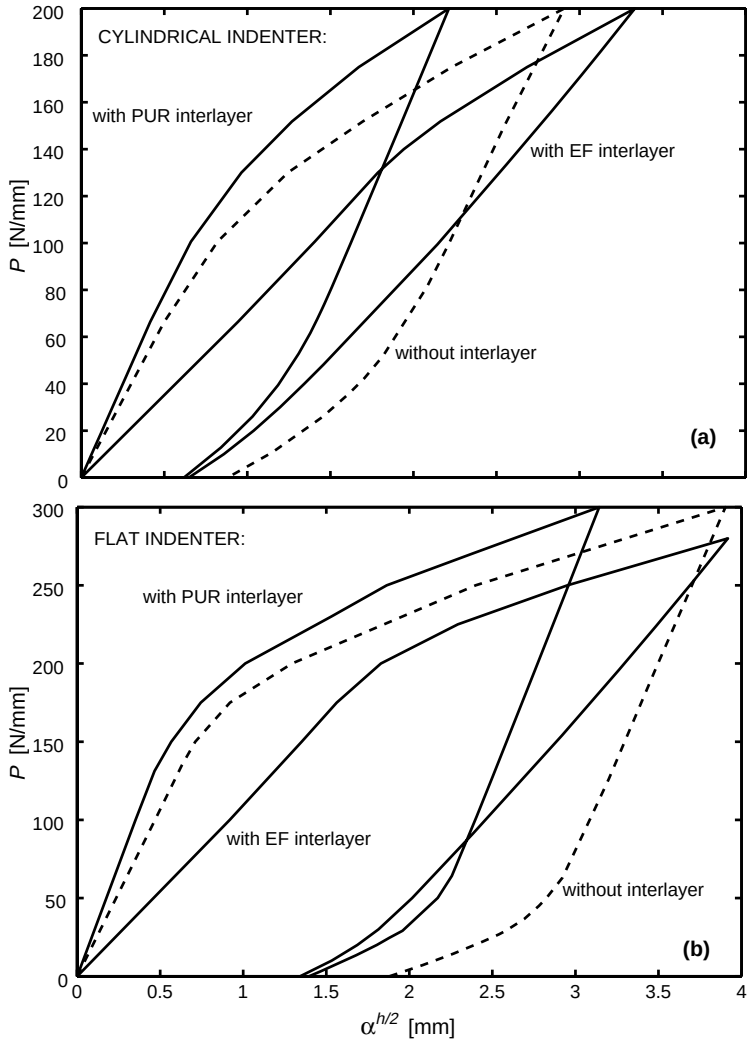

Fig. 4. Force-skin indentation relationship for sandwich plates with or without an interlayer, impacted by a cylindrical or a flat indenter; absence of interfacial crack is assumed.

candidate materials and sandwich plate thicknesses. The implication is that both high interlayer thickness and modulus reduce interface deflections, and thus delay onset of crushing of the foam core. Interlayer thickness has a significant effect on deflection magnitude even at high modulus values, where the influence of interlayer stiffness is much reduced.

3.3. Local stresses caused by the indenters

The two stress components that affect structural integrity of the plate are the normal stress σ_z^{int} at the interface with the foam core, and the tension stress σ_x^{int} caused by the indenter at the bottom surface ($z = h/2 - t_f$) of the top face sheet. The stress σ_x^{int} is found for a homogenized laminate layer. Actual ply stresses can be derived from corresponding strains and ply orientations.

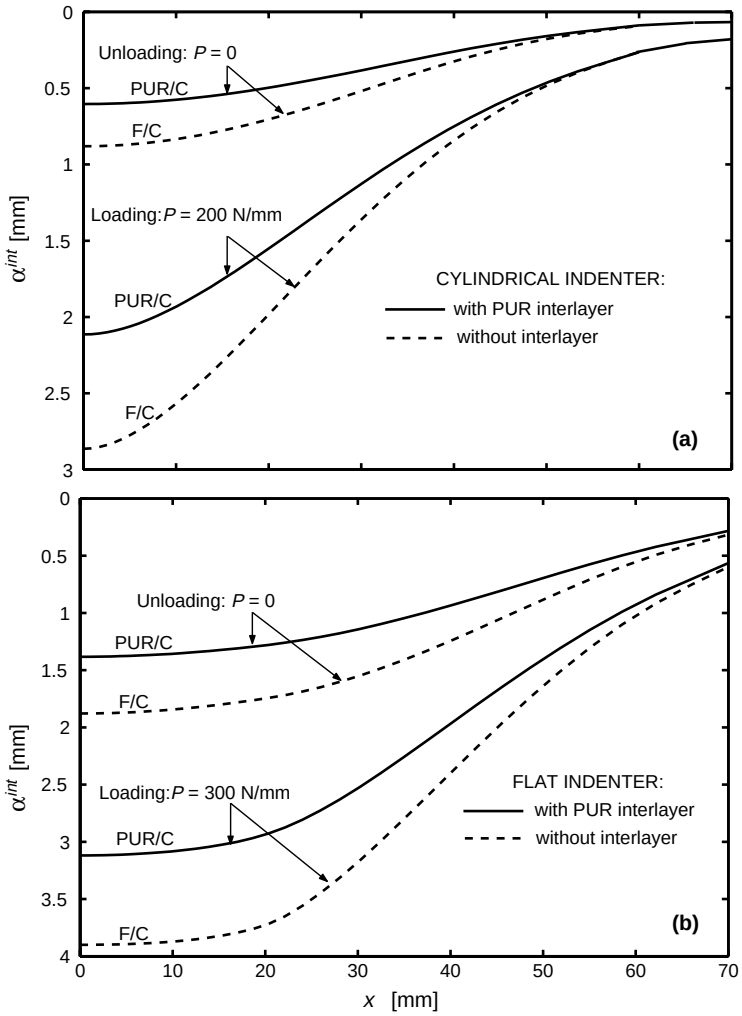

Fig. 5. Deflection distribution at the foam core interface in a sandwich plate with or without an interlayer. Forces applied to the cylindrical or flat indenters are $P = 200\,\mathrm{N/mm}$ or $300\,\mathrm{N/mm}$, respectively.

As seen in Fig. 7, the magnitude of σ_z^{int} at maximum load of $200\,\mathrm{N/mm}$ is not too sensitive to indenter shape, especially in the presence of the PUR interlayer. This is consistent with the rather low hardening rate observed and prescribed during crushing of the foam core. Upon unloading to $P = 0$, existence of the permanent strain in the foam core gives rise to residual stresses. Under loading/unloading by the cylindrical indenter, the residual stress σ_z^{int} becomes positive over a fairly large area. This is followed by a relatively steep change to a compressive residual stress, which then decreases to zero at a larger distance. Unloading of the flat indenter from the same maximum load of $P = 200\,\mathrm{N/mm}$ also generates high residual stresses in the vicinity of the end corner of the indenter. These residual stresses can drive interfacial cracks, as discussed in Section 4 below.

Penetration of the face sheet by an indenter represents another failure mechanism that may be caused by low velocity impact. The risk can be estimated by evaluating the normal stress σ_x^{int} in the face sheet. Fig. 8 shows the distribution of these stresses with the distance x from the centers of two indenters. For

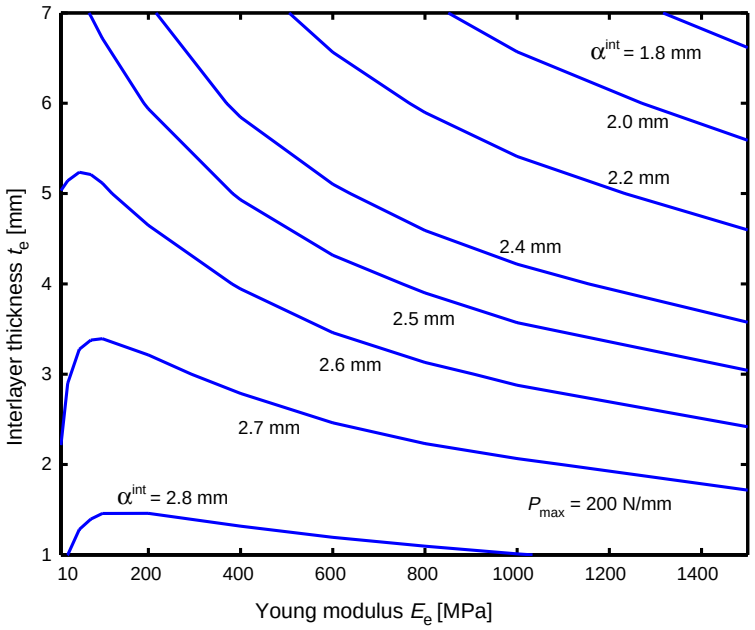

Fig. 6. Deflection of the foam core interface protected by an incompressible interlayer with Young's modulus E_e and thickness t_e; the Poisson's ratio $\nu_e = 0.49$. The load applied to the cylindrical indenter is $P_{max} = 200\,\mathrm{N/mm}$.

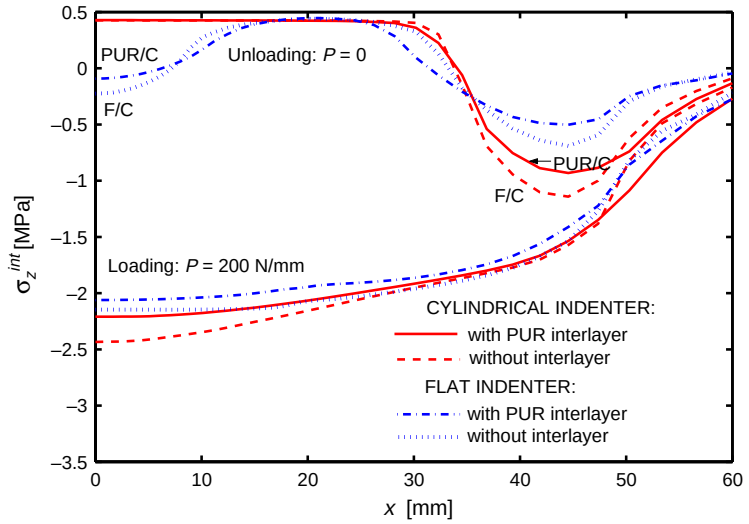

Fig. 7. Normal stress distribution at the interface with foam core in a sandwich plate with or without an interlayer, impacted by a cylindrical or a flat indenter; applied force $P = 200\,\mathrm{N/mm}$.

the cylindrical indenter, the maximum values are found at the center $x = 0$ of the contact zone. The maxima caused by the flat indenter are found in the vicinity of the corner at $x = 20\,\mathrm{mm}$, c.f., Fig. 3. For both indenter shapes, the stiff PUR interface offers a significant reduction of the face sheet stress.

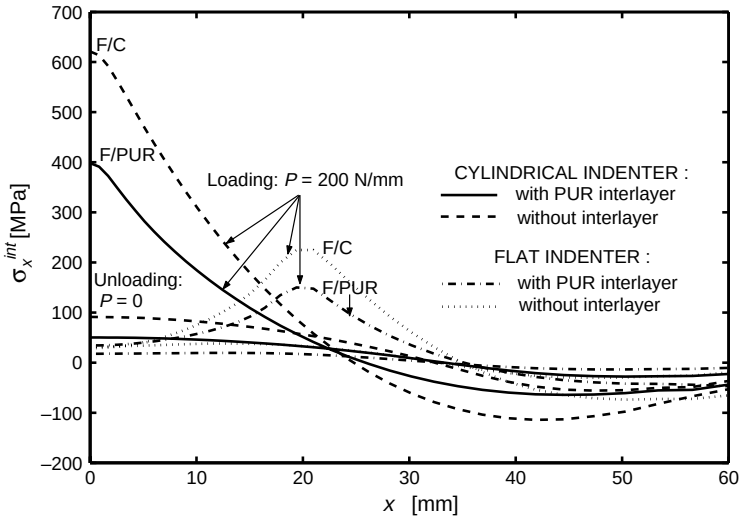

Fig. 8. Distribution of the stress σ_x^{int} in the top face sheet ($z = h/2 - t_f$) at the interface with the foam core C, or PUR interlayer, for a sandwich plate impacted by a cylindrical or a flat indenter; applied force $P = 200\,\text{N/mm}$.

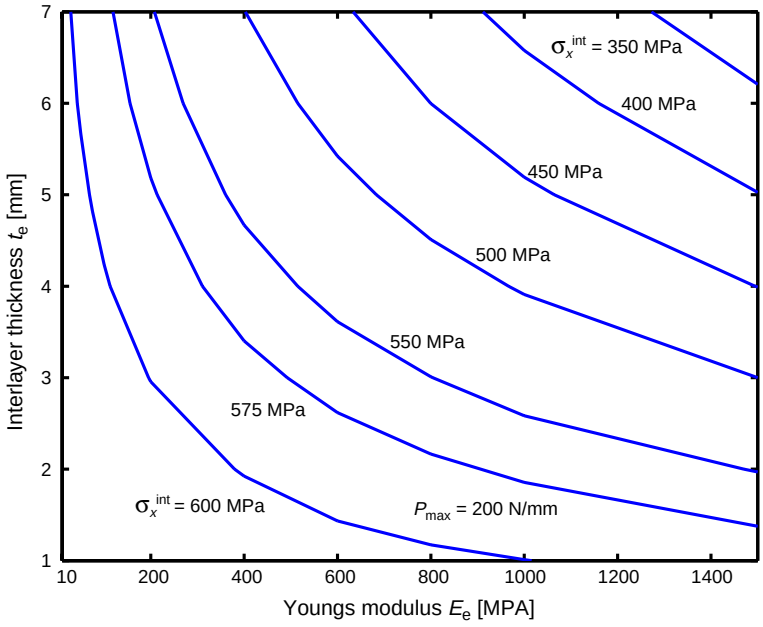

Fig. 9. Tensile stress σ_x^{int} in the face sheet at $z = h/2 - t_f$, supported by an incompressible interlayer as a function of the Young's modulus E_e and the thickness t_e of the interlayer; the Poisson's ratio $\nu_e = 0.49$. The load applied to the cylindrical indenter is $P_{\max} = 200\,\text{N/mm}$.

The relative effect of the interlayer thickness and elastic modulus on the face sheet normal stress is illustrated in Fig. 9. The overall trend is similar to that shown in Fig. 6, but an increase in interlayer stiffness appears to have a stronger influence on the face sheet stress reduction.

3.4. Effect of impact velocity on loads and deflections

Dynamic response of the sandwich plate was evaluated with an implicit direct-integration dynamic operator, or the α-method of Hilber et al. (1978), Chung and Hulbert (1993), implemented in the ABAQUS software. To illustrate the impact velocity effect on deflection and contact force magnitudes and rates, a cylindrical indenter with mass $m = 0.06$ kg/mm per unit y-direction length was applied to several sandwich plate configurations at velocities of 1–3 m/s. The deceleration of the indenter by the plate was converted into a time-dependent contact force P, using,

$$P = -ma_z = -m\frac{\mathrm{d}^2 w}{\mathrm{d}t^2} \tag{10}$$

where a_z is the acceleration and w is the displacement of the center of mass of the indenter. Since the indentation problem utilizes symmetry with respect to both the $x = 0$ and $y = 0$ planes, the a_z is the only nonzero acceleration component. P is the resultant of all forces imposed by the decelerating indenter on the top face sheet.

Fig. 10 shows deflections $\alpha^{h/2}$ of the top face sheet F, and α^{int} of foam core interface with the top face sheet F, or PUR and EF interlayers. The indenter velocity is 3 m/s. The deflection rates are comparable to the impact velocity, of the order of 1 m/s. The dashed lines show the surface and F/C interface deflections in a conventionally designed plate. The two adjacent solid lines indicate that the stiff PUR interlayer causes a small reduction of both these deflections. The most striking but not unexpected result is found for the plate with the compressible EF interlayer, where the face sheet deflection is much higher than in the conventionally designed plate, while the foam core deflection has been much reduced. This result illustrates the protection that the EF interlayer offers to the foam core, while it withholds support of the top face sheet.

Fig. 11 shows magnitudes of contact forces P generated in different plate configurations by the indenter mass used in Fig. 10 approaching the top face sheet at several impact velocities. Again, the dashed lines apply to the conventionally designed plate. Increasing the impact velocity V from 1 to 3 m/s has a significant

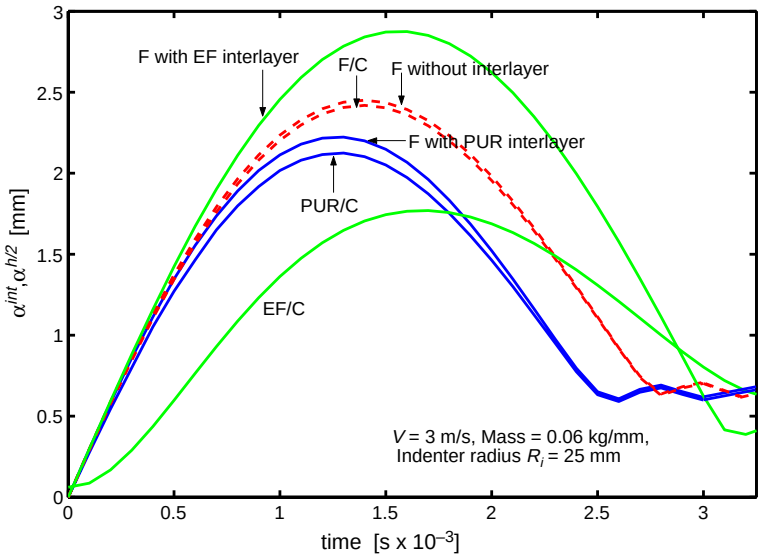

Fig. 10. Deflection at the interface with foam core α^{int} and a top face sheet indentation $\alpha^{h/2}$ for a sandwich plate with or without interlayer impacted by a cylindrical indenter of radius $R_i = 25$ mm.

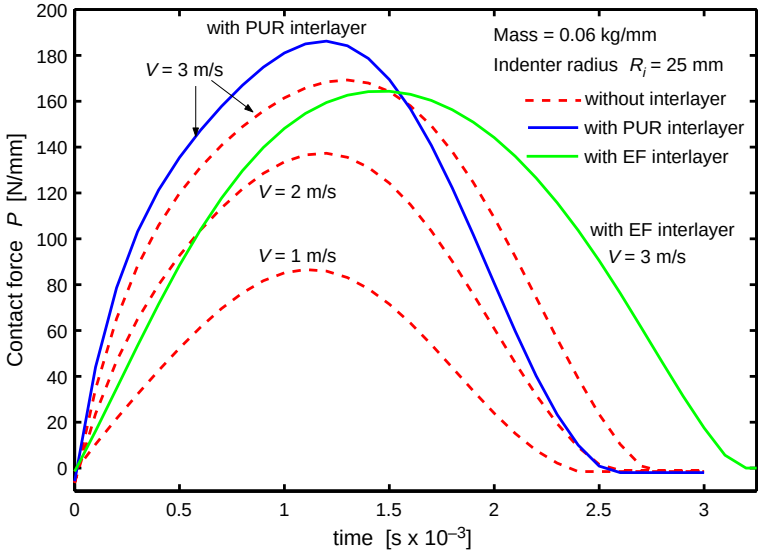

Fig. 11. Contact force P exerted on the sandwich plate with or without interlayer for different velocities of the cylindrical indenter of radius $R_i = 25\,\text{mm}$.

effect, raising the contact force maximum from 80 to 170 N/mm, or by more than 100%. The two solid lines were both found at impact velocity $V = 3\,\text{m/s}$, for plates with either PUR or EF interlayers. The stiff interlayer tends to elevate both the contact force maximum and the loading rate. On the other hand, both the load and its rate are reduced in plates with the compressible EF interlayer.

Approximate values of strain rate magnitudes in the foam or PUR and EF interlayers can be deduced from the results in Fig. 11. For example, at $V = 3\,\text{m/s}$, the time to reach $P = 190\,\text{N/mm}$ is approximately equal to $1.2 \times 10^{-3}\,\text{s}$. As seen in Fig. 7, the stress caused at the PUR/foam core interface for the load $P = 200\,\text{N/mm}$ is $\sigma_z^{\text{int}} \approx -2.2$ MPa. This suggests the stress rate of about 1833 MPa/s. Dividing this by the foam core modulus $E_c = 111\,\text{MPa}$ gives the strain rate of $16.5\,\text{s}^{-1}$. For the PUR interlayer, with $E_e = 1500\,\text{MPa}$, the strain rate is equal to $1.22\,\text{s}^{-1}$. Therefore, the local strain rates to be expected at impact velocities of the order of 1–10 m/s are of the order of $1\text{–}100\,\text{s}^{-1}$, depending on the local material stiffness.

The properties of the layers constituting the sandwich plate can be affected at these high loading rates. The dependence on the strain rate of the elastic moduli of the PUR interlayer at temperatures below the glass transition temperature $T < T_g \approx 100\,^\circ\text{C}$ is very small and can be neglected (Gibson and Ashby, 1997). The same is true for the PVC foam core since the foam inherits the strain-rate and temperature dependence of the solid of the cell walls (Thomas et al., 2003). However, some dependence of the compressive strength σ_c^0 of the foam on the strain-rate has been observed even at room temperatures. In particular (Gibson and Ashby, 1997),

$$\sigma_c^0/\bar{\sigma}_c^0 = 1 - 0.1\frac{T}{T_g}\ln\frac{10^4}{\dot{\epsilon}} \tag{11}$$

where $\bar{\sigma}_c^0$ is the strength at 0 K. Assuming $\dot{\epsilon} = 16.5$, $T = 20\,^\circ\text{C}$ gives $\sigma_c^0 = 0.872\bar{\sigma}_c^0$, and for $\dot{\epsilon} = 10^{-2}$ $\sigma_c^0 = 0.723\bar{\sigma}_c^0$. Thus the compressive strength grows with the increase of the strain rate. The growth of compressive strength at higher strain rates (or impact velocities) can be explained, in part, by the tighter compression of the cell walls near the impact zone, which results in densification of the foam and consequently an increase of the crushing stress.

For the EF interlayer, however, $T_g \approx -70\,^{\circ}\mathrm{C}$ is now below the room temperature and dependence of both the elastic moduli E_e and the compressive strength of the foam on the strain rate is expected. Both the elastic moduli and the compressive strength grow with the increase of the strain rate. However, this dependence appears to be pronounced for elastomeric foam of low densities of the order $\rho = 10$–$50\,\mathrm{kg/m^3}$. These foams have low Young's modulus E_e of the order of 0.1–1 MPa and an addition of 0.1 MPa caused by the atmospheric pressure of gas inside the cells of the foam can not be neglected. In the present study, the Young's modulus of the EF was chosen as $E_e = 10\,\mathrm{MPa}$, so the atmospheric pressure of gas can be disregarded.

In summary, neglecting strain rate effects is justified for the materials and loading conditions selected herein. However, such effects may become significant in other interlayer and core materials, or under higher temperatures and loading rates.

4. Energy released by interfacial cracks

Crushing of the foam core and the resulting residual stresses at interfaces with the foam core and face sheet can impair the strength of the interfacial bond and initiate interfacial cracks that may then extend, e.g., under cyclic service loads, and cause extensive internal delamination of the sandwich plate. The propensity to interfacial cracking is estimated here by evaluating the energy release rate G by interfacial cracks driven only by the residual stresses during the last stage of unloading, when the resolved normal stress across the particular interface changes from compression to tension. In the figures that follow, G was found at several selected load levels P_u on the loading/unloading diagram.

The energy release rate G is evaluated here by two well known methods, by the crack closure integral and by the J-integral. Both are computed using the crack tips fields obtained from finite element analysis. Fig. 12 shows the refined mesh used for cracks at the interfaces PUR/C or EF/C between the two interlayers and foam core C. Similar refinements were used for cracks at F/C and F/PUR, F/EF interfaces between face sheet F and foam core C, or face sheet and interlayers. The actual crack length was changed at regular intervals that are indicated in the related Figs. 13–15.

The crack closure integral evaluation of G assumes purely elastic response of the materials adjoining the crack tip. That was enforced by elevating the tensile strength of the foam core in tension σ_t^0 and thus avoiding inelastic deformation during unloading. This can introduce only a small error into the solution since the possible change of the plastic strains during unloading, arising under assumption of inelastic response of the foam, occurs only in a very small region near the crack tip. The energy released by an incremental crack extension can then be estimated from the work of surface tractions on the crack opening displacements, required to close the crack extension increment. This is written as

$$G = \lim_{\Delta a \to 0} \frac{1}{\Delta a} \int_0^{\Delta a} [\sigma_{33}(s)\Delta u_3(\Delta a - s) + \sigma_{31}(s)\Delta u_1(\Delta a - s)]\,\mathrm{d}s \tag{12}$$

where Δa is the crack extension increment, σ_{3i} are stress components ahead of the crack tip that correspond to traction components on the faces of an open crack, and Δu_i are the crack opening displacements.

Since accurate stress values are obtained only at integration points of each finite element, derivation of the resolved stresses on the crack line is facilitated by estimating the order of the crack tip singularity. For a crack propagating along the interface between two isotropic elastic solids, the stresses ahead of the crack tip are given by

$$\sigma_{33} = \mathrm{Re}[Kr^{i\epsilon}](2\pi r)^{-1/2} \quad \sigma_{13} = \mathrm{Im}[Kr^{i\epsilon}](2\pi r)^{-1/2} \tag{13}$$

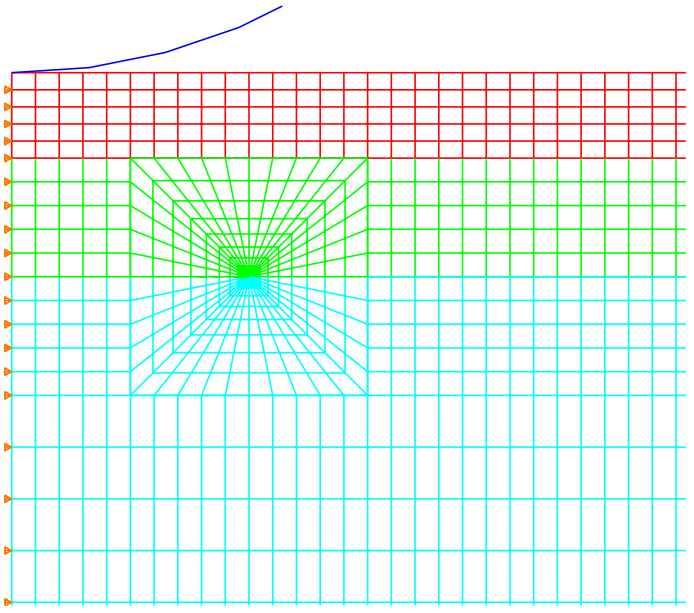

Fig. 12. Refinement of the finite element mesh at the crack tip.

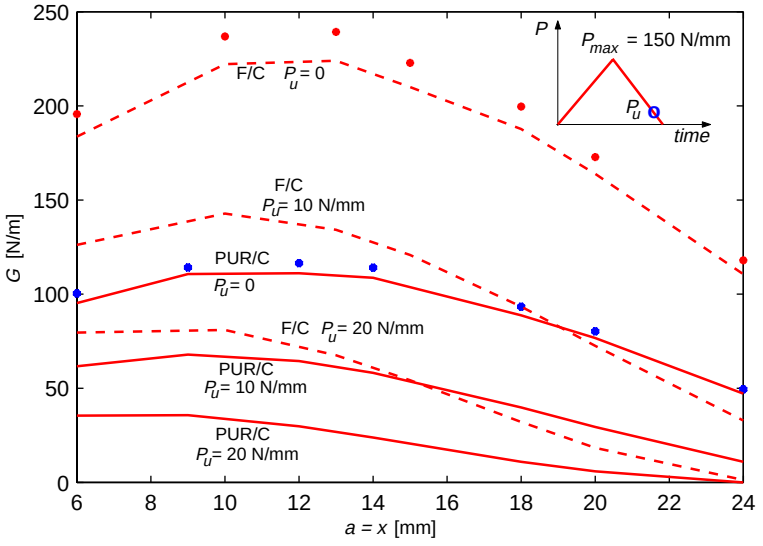

Fig. 13. Energy release rate G versus half of the crack length a for $P_{\max} = 150\,\mathrm{N/mm}$ applied to the cylindrical indenter; the crack extends at the interface with the foam core. Points and lines represent G found from crack closure, and J integrals, respectively.

where $K = K_1 + iK_2$ is the complex stress intensity factor, and $\epsilon = \ln((1-\beta)/(1+\beta))/(2\pi)$ is a parameter measuring mismatch between the elastic moduli of the two solids, β is a Dundurs parameter (Hutchinson and Suo, 1992). The square root singularity dominates the solution (13) because ϵ is a small number. For example, for the interface between the foam core and PUR interlayer $\epsilon = 0.144$, and for the interface between the foam core and the elastomeric foam interlayer $\epsilon = 0.1438$. This suggests that the parameter ϵ

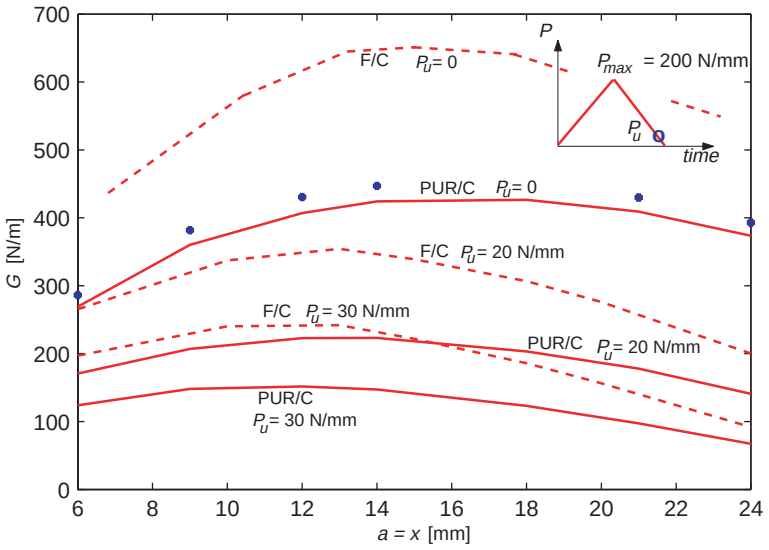

Fig. 14. Energy release rate G versus half of the crack length a for $P_{\max} = 200\,\mathrm{N/mm}$ applied to the cylindrical indenter; the crack extends at the interface with the foam core. Points and lines represent G found from crack closure, and J integrals, respectively.

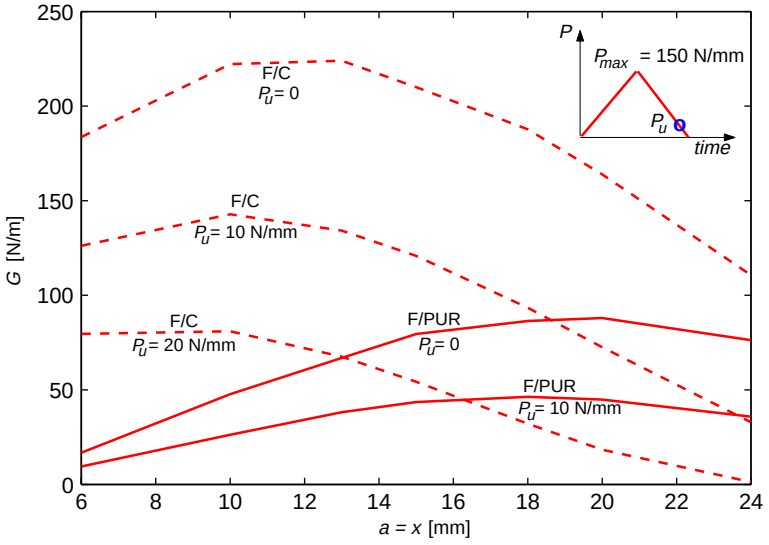

Fig. 15. Energy release rate G versus half of the crack length a for $P_{\max} = 150\,\mathrm{N/mm}$ applied to the cylindrical indenter; the crack extends at the interface with the face sheet.

can be neglected. As shown by Qu and Bassani (1989), the inverse square root singularity also prevails under the present loading conditions between the orthotropic face sheet and an isotropic substrate.

This enables use of crack tip elements that reproduce exactly the $r^{-1/2}$ singularity in crack tip stresses and strains. The stresses and crack opening displacements near the crack tip can then be represented by

$$\sigma_{3i} = \frac{k_s^i}{\sqrt{s}}, \quad u_i = k_u^i \sqrt{\Delta a - s} \tag{14}$$

where k_s and k_u are yet unknown coefficients that can be estimated from the finite element solution.

Then, (12) is written as

$$G = \frac{k_s^3 k_u^3 + k_s^1 k_u^1}{2\Delta a} \int_0^{\Delta a} \frac{\sqrt{\Delta a - s}}{\sqrt{s}} \, \mathrm{d}s = \frac{k_s^3 k_u^3 + k_s^1 k_u^1}{2\Delta a} \frac{\pi \Delta a}{2} \tag{15}$$

so that the energy release rate becomes

$$G = \frac{\pi(k_s^3 k_u^3 + k_s^1 k_u^1)}{4} \tag{16}$$

To find coefficients k_s and k_u one can consider solution at the ring of collapsed quadrilateral elements adjoining the crack tip, Fig. 12. Radius of that ring of elements was 0.05 mm. In particular, the stresses in the element touching the interface and located ahead of the crack tip can be used to find the coefficient k_s. The most accurate stress values are obtained at nine integration points of the element. The stresses at three integration points having the common natural coordinate, say $\eta = 0$, and located approximately at $l/4$ distance from the crack tip O ($l = 0.05$ mm is the size of the element) can be extrapolated to the "mid-side" nodes having the same natural coordinate $\eta = 0$. Since this extrapolation takes place in a nonsingular circumferential direction around the crack tip, the stresses at the midside nodes are considered to be more accurate than those extrapolated to corner nodes.

If σ is the stress at the midside node, then from (14) (neglecting indices),

$$k_s = \sigma \sqrt{\frac{l}{4}} \tag{17}$$

The k_u are derived from crack opening displacements at a pair of nodes equally located behind the crack tip O,

$$k_u = \frac{\Delta u}{\sqrt{l}} \quad \text{or} \quad k_u = \frac{\Delta u}{\sqrt{l/4}} \tag{18}$$

where in the first formula Δu is the opening displacement of the corner nodes, and in the second formula Δu is the opening displacement of the midside nodes.

The energy release rate for a crack propagating in the x-direction can also be evaluated as the J-integral,

$$J = \int_\Gamma (W \delta_{1j} - \sigma_{ij} u_{i,1}) n_j \, \mathrm{d}\Gamma \tag{19}$$

where Γ is a contour surrounding the crack tip, W is the strain energy, and n_j are components of the outward normal vector to Γ. The strain energy is defined as

$$W = \int \sigma_{ij} \, \mathrm{d}\epsilon_{ij} = \int \sigma_{ij} (\mathrm{d}\epsilon_{ij}^e + \mathrm{d}\epsilon_{ij}^p) \tag{20}$$

where both elastic and inelastic strains, estimated in the J-integral by the deformation plasticity theory, are included. As noted by Moran and Shih (1987), the presence of thermal or residual stresses renders the J-integral globally path-dependent. However, path-independence is restored if the Γ-contour is sufficiently small. In the present evaluation, Γ coincides with the outer boundary of the second ring of elements surrounding the crack tip, which has the radius of 0.25 mm.

Results of the strain energy release rate calculations for cracks driven by the residual stresses at interfaces inside the sandwich plate are shown in Figs. 13–15 for different maximum load magnitudes $P_{\max}$

applied to the cylindrical indenter. As noted earlier, cracking follows unloading from a selected value of P_{max}, and the energy release rate is monitored here at load levels $P = P_u$, when G reaches reasonably large magnitudes.

The release rates are evaluated for single cracks of increasing length $2a$ that have been extended symmetrically in the $\pm x$-direction on a certain interface, using meshes of the kind indicated in Fig. 12. Figs. 13 and 15 show the release rates for unloading from $P_{max} = 150\,\text{N/mm}$, and Fig. 14 shows results for unloading from $P_{max} = 200\,\text{N/mm}$.

The plotted curves have a positive slope at small crack lengths, reach a maximum value at $a = 10$–$12\,\text{mm}$ (or 16–18 mm), and then decline as the crack half-length grows. This is consistent with the residual stress distributions after unloading in Fig. 7. The dashed lines in Figs. 13–15 indicate magnitudes of energy release rate G for cracks extending along the F/C interface between the face sheet and foam core in a conventionally designed plate of Fig. 1a. As the applied load is reduced from $P_u = 20\,\text{N/mm}$ (or 30 N/mm) to $P_u = 0$, the magnitude of G grows substantially. The solid lines indicate magnitudes of G computed for cracks extending at the interface PUR/C between the stiff polyurethane interlayer and the foam core (Figs. 13 and 14) and the interface F/PUR between the face sheet and polyurethane interlayer (Fig. 15). These are much lower than those found at the F/C interface, and the difference grows as $P \to 0$.

In summary, the values of G found at the PUR/C and F/PUR interfaces are much lower than those at the F/C interface.

Table 4 compares the values of energy release rates G, evaluated from finite element solution as the J-integrals, for different designs of the sandwich plate (without interlayer, and with PUR or EF interlayers) loaded by a cylindrical indenter. The Gs are given at the interface with the foam core at the final stage of unloading, i.e., $P_u = 0$, from the maximum load $P_{max} = 200\,\text{N/mm}$, and at the interface with the face sheet at $P_u = 0$ when $P_{max} = 150\,\text{N/mm}$. The results clearly illustrate the principal benefit provided by the presence of the interlayer: reduction of the interfacial crack driving forces derived from residual stresses generated by inelastic deformation caused by low-velocity impact. While the elastomeric foam (EF) interlayer offers greater reduction of G, it lacks the stiffness sufficient for maintaining small plate and face sheet deflections under distributed and concentrated loads.

Table 5 shows the values of debond fracture toughnesses G_c reported by several investigators at the interface between the face sheet and foam core for conventionally designed sandwich plates. All values have been obtained by performing double cantilever beam tests at room temperatures with no exposure to sea environment. The foam core had no residual stresses and was not crushed. In Berkowitz et al. (2003) the beam specimens with the crack cut with a saw between one face sheet and the core had been loaded by tensile forces via piano hinges riveted to the face sheets. The loading rate was low; the corresponding displacement rate of the hinges was only 0.0212 mm/s. Bazant et al. (in press) measured the fracture toughness of

Table 4
Energy release rates G (N/m), for various designs of sandwich plate loaded by a cylindrical indenter at the interfaces with the foam core C and the face sheet F

Crack length $2a$ (mm)	F/C	PUR/C	EF/C
$P_{max} = 200\,\text{N/mm}$, $P_u = 0$			
16	508	330	245
20	583	376	249
		F/PUR	F/EF
$P_{max} = 150\,\text{N/mm}$, $P_u = 0$			
16	203	32	25
20	222	48	25
36	188	86	11

Table 5
The values of debond fracture toughness G (N/m), for the face sheet—foam core interface in a conventionally designed sandwich plates

Foam core	Face sheet	G_c (N/m)	References
H100 PVC	Composite	500	Li and Weitsman (2003)
H130 PVC	E-glass/vinyl ester	≈900	Veazie et al. (2003)
Nomex honeycomb	Graphite/epoxy	1177	Berkowitz et al. (2003)
H100 PVC	Carbon-fabric/epoxy	≈700	Shivakumar et al. (2003)

the Divinycell H100 foam using the size effect method. The value of G_c of the foam reported in that paper was 490 N/m.

Comparison of the fracture toughnesses (Table 5) with the energy release rates G in Figs. 13–15 and Table 4, especially at high loads $P_{max} = 200$ N/mm, leads to the conclusion that the energy release rates G may exceed the toughness G_c. This can cause an interface cracking in a conventionally designed plates. This is especially true for the sandwich plate impacted by the indenter since the value of toughness G_c can be expected to be lower than that indicated in Table 5 due to crushing of the foam core. Also, the values of energy release rates G can be higher than those in Figs. 13–15 if the foam core with lower hardening is selected in the sandwich plate design.

However, the interface cracking can be prevented if the interlayer is inserted between the face sheet and the foam core.

5. Conclusions

Response of several sandwich plate designs to uniformly distributed loads and to a quasi-static simulation of a low velocity impact by rigid indenters has been evaluated and compared. Conventionally designed plates consisting of laminated composite face sheets and PVC foam core have been analyzed together with similar plates containing one of two different ductile interlayers, bonded between the top face sheet and the foam core of correspondingly reduced thickness. By separating the foam core from the impacted face sheet, the interlayers absorb most of its deflection and thus reduce the extent of local foam core crushing. Therefore, the residual strains that drive interface cracks after unloading are significantly reduced.

Two interlayer materials with distinctly different stiffness and compressibility were examined with regard to their effect on overall deflection of the plate in service, and on the laminated face sheet deflection and fiber stresses under impact loads, a relatively stiff, incompressible and very ductile polyurethane (PUR), and a compliant and compressible elastomeric foam (EF).

Comparisons of overall bending deflections and impact damage resistance show that the design modifications analyzed herein offer a substantial benefit. The stiff and incompressible PUR interlayer, bonded to the external face sheet and the underlying foam core, reduces both overall deflections of the plate under a given distributed load, and the face sheet and core interface deflections under a prescribed concentrated load. The residual stresses that provide a driving force for interfacial cracks are also lower than those in the conventionally designed sandwich plate.

Exchanging the PUR interlayer for the compliant and compressible elastomeric foam (EF) interlayer while keeping applied loads constant, elevates both overall plate deflections and local deflections and in-plane normal stress in the face sheet. The magnitude of these changes is suggested by Figs. 6 and 9, where the EF interlayer response can be read at $E_e = 10$ MPa, and that of the PUR interlayer at $E_e = 1500$ MPa. However, the contact force imparted by a given kinetic energy to the plate with an EF interlayer is lower than that found in a plate with the PUR interlayer (Fig. 11), resulting in lower deflections. Using somewhat thicker face sheets would further limit the said deflections and also complement the already significant effect

of the EF interlayer on reduction of permanent compression of the foam core and the interfacial crack driving forces derived from residual stresses.

More extensive comparisons of the relative merits of different sandwich plate designs are needed under other loads and constraints that may be applied to the sandwich plates in service. Since the results provide only the deformation and stress fields, and the driving forces for interfacial cracks, their implementation in design would need to be augmented by measurement of local toughness magnitudes for cracks extending along or in close proximity to the interfaces in the selected plate materials. Fabrication procedures for the sandwich plates with interlayers and related expenses also need to be considered in actual applications of the proposed design modifications. Some of these issues will be addressed in future work.

Acknowledgement

The authors gratefully acknowledge the support provided by the Office of Naval Research. Dr. Yapa D.S. Rajapakse served as program monitor.

Appendix A

The constitutive equation for orthotropic material can be written as

$$\begin{aligned}&\boldsymbol{\sigma} = \boldsymbol{L}\boldsymbol{\epsilon}\\ &\boldsymbol{\sigma} = \{\sigma_{11}\sigma_{22}\sigma_{33}\sigma_{23}\sigma_{13}\sigma_{12}\}^{\mathrm{T}}, \quad \boldsymbol{\epsilon} = \{\epsilon_{11}\epsilon_{22}\epsilon_{33}2\epsilon_{23}2\epsilon_{13}2\epsilon_{12}\}^{\mathrm{T}}\end{aligned} \tag{A.1}$$

with nonzero coefficients of stiffness matrix $\boldsymbol{L}$ given by (Herakovich, 1998),

$$\begin{aligned}&L_{11} = \frac{1-v_{23}v_{32}}{E_2E_3\Delta}, \qquad L_{22} = \frac{1-v_{13}v_{31}}{E_1E_3\Delta}, \qquad L_{33} = \frac{1-v_{12}v_{21}}{E_1E_2\Delta}\\ &L_{12} = L_{21} = \frac{v_{21}+v_{23}v_{31}}{E_2E_3\Delta}, \qquad L_{13} = L_{31} = \frac{v_{31}+v_{21}v_{32}}{E_2E_3\Delta}, \qquad L_{23} = L_{32} = \frac{v_{32}+v_{12}v_{31}}{E_1E_3\Delta}\\ &L_{44} = G_{23}, \qquad L_{55} = G_{13}, \qquad L_{66} = G_{12}\\ &\Delta = (1-v_{12}v_{21}-v_{23}v_{32}-v_{13}v_{31}-2v_{21}v_{32}v_{13})/(E_1E_2E_3)\end{aligned} \tag{A.2}$$

The following connections between elastic constants hold:

$$\frac{v_{13}}{E_1} = \frac{v_{31}}{E_3}, \qquad \frac{v_{23}}{E_2} = \frac{v_{32}}{E_3}, \qquad \frac{v_{12}}{E_1} = \frac{v_{21}}{E_2} \tag{A.3}$$

The subscripts correspond to coordinate axes $x_1 = x$, $x_2 = y$, and $x_3 = z$.

Appendix B

In the elastic region, the foam is modeled as linear isotropic material, Table 1. The plastic part of the behavior is defined by the crushable foam model provided by ABAQUS. The yield surface is a circle in the deviatoric stress plane and an ellipse in the meridional $p-q$ stress plane, where p is the mean pressure,

$$p = -\frac{1}{3}(\sigma_{11}+\sigma_{22}+\sigma_{33}) \tag{B.1}$$

and q is the Mises stress,

$$q = \sqrt{\frac{3}{2}s_{ij}s_{ij}}, \quad s_{ij} = \sigma_{ij} + p\delta_{ij} \tag{B.2}$$

The volumetric hardening model is used where the point of the yield ellipse that represents pure hydrostatic tension loading is fixed, and the evolution of the yield surface is driven by the volumetric compacting plastic strain. The yield surface is defined as

$$F = \sqrt{q^2 + \alpha^2\left(p - \left(\frac{p_c - p_t}{2}\right)\right)^2} - \alpha\frac{p_c + p_t}{2} = 0 \tag{B.3}$$

where p_t is the strength of the material in hydrostatic tension (fixed), p_c is the strength of the material in hydrostatic compression, α is the shape factor that defines the relative magnitude of the p and q axes. The shape factor is defined as

$$\alpha = \frac{3k}{\sqrt{(3k_t + k)(3 - k)}}, \quad k = \frac{\sigma_c^0}{p_c^0}, \quad k_t = \frac{p_t}{p_c^0} \tag{B.4}$$

where p_c^0 is the initial yield stress in hydrostatic compression, σ_c^0 is the initial yield stress in uniaxial compression. Usually $k_t \approx 0.1$, $k \approx 1$.

The compressive strength p_c evolves as a result of compaction (increase in density). Evolution of the yield surface is expressed through a change of the yield surface size $p_c + p_t$ along the hydrostatic ($q = 0$) stress axis, as a function of the value of volumetric compacting plastic strain $-\epsilon_{vol}^{pl}$. This function is given by

$$p_c(\epsilon_{vol}^{pl}) = \frac{\sigma_c(\epsilon_a^{pl})[\sigma_c(\epsilon_a^{pl})(1/\alpha^2 + 1/9) + p_t/3]}{p_t + \sigma_c(\epsilon_a^{pl})/3} \tag{B.5}$$

where ϵ_a^{pl} is the axial plastic strain, and σ_c is the yield stress in uniaxial compression test. For the present analysis, the function $\sigma_c(\epsilon_a^{pl})$ was obtained from (5). In uniaxial compression, $\epsilon_{vol}^{pl} = \epsilon_a^{pl}$ for the volumetric hardening model.

The flow potential is given by

$$Q = \sqrt{q^2 + \frac{9}{2}p^2} \tag{B.6}$$

The equivalent plastic strain rate is defined as

$$\dot{\bar{\epsilon}}_{pl} = \frac{1}{Q}\sigma_{ij}\dot{\epsilon}_{ij}^{pl} \tag{B.7}$$

and the plastic strain rate is assumed to be

$$\dot{\epsilon}_{ij}^{pl} = \dot{\bar{\epsilon}}_{pl}\frac{\partial Q}{\partial \sigma_{ij}}. \tag{B.8}$$

References

ABAQUS, Version 6.2., 2001. Hibbit, Karlsson and Sorenson, Inc., Pawtucket, RI.

Barovich, D., Kingsley, S.C., Ku, T.C., 1964. Stresses on a thin strip or slab with different elastic properties from that of the substrate due to elliptically distributed load. International Journal of Engineering Sciences 2, 253.

Bazant, Z.P., Zhou, Y., Zi, G., Daniel, I.M., in press. Size effect and asymptotic analysis of fracture of closed-cell polymeric foam. International Journal of Solids and Structures.

Berkowitz, C.K., Johnson, W.S., Makeev, A., 2003. Environmental effects on the fatigue and fracture of Nomex honeycomb sandwich structure. in: Proceedings of the 6th International Conference on Sandwich Structures, pp. 496–510.

Blatz, P.J., 1971. On the thermostatic behavior of elastomers. In: Polymer Networks, Structure and Mechanical Properties. Plenum Press, New York, pp. 23–45.

Chung, L., Hulbert, G., 1993. A time integration algorithm for structural dynamics with improved numerical dissipation; the generalized α-method. Journal of Applied Mechanics 60, 371–375.

Dvorak, G.J., Suvorov, A.P., in press. Protection of sandwich plates from low velocity impact. Journal of Composite Materials, 38.

Gibson, L.J., Ashby, M.F., 1997. Cellular Solids: Structures and Properties, second ed. Cambridge University Press.

Gudmundson, P., Zang, W., 1993. An analytic model for thermoelastic properties of composite laminates containing transverse matrix cracks. International Journal of Solids and Structures 30 (23), 3211–3231.

Gupta, P.K., Walowit, J.A., Finkin, E.F., 1973. Stress distributions in plane strain layered elastic solids subjected to arbitrary boundary loading. Journal of Lubrication Technology, 427–432.

Herakovich, C.T., 1998. Mechanics of fibrous composites. John Wiley and Sons, Inc., New York.

Hilber, H.M., Hughes, T.J.R., Taylor, R.L., 1978. Collocation, dissipation and 'overshoot' for time integration schemes in structural dynamics. Earthquake Engineering and Structural Dynamics 6, 99–117.

Hutchinson, J.W., Suo, Z., 1992. Mixed mode cracking in layered materials. Advances in Applied Mechanics 29, 63–191.

Johnson, K.L., 1987. Contact Mechanics. Cambridge University Press, New York.

Lee, L.J., Huang, K.Y., Fann, Y.J., 1993. Dynamic responses of composite sandwich plate impacted by a rigid ball. Journal of Composite Materials 27, 1238–1256.

Li, X., Weitsman, J., 2003. Sea water effects on foam-cored composite sandwich layups, in: Proceedings of the 6th International Conference on Sandwich Structures, pp. 443–455.

Lindholm, C.J., Abrahamsson, P., 2003. Modelling and testing of the indentation behavior of sandwich panels subject to localized load, in: Proceedings of the 6th International Conference on Sandwich Structures, pp. 279–291.

Moran, B., Shih, C.F., 1987. Crack tip and associated domain integrals from momentum and energy balance. Engineering Fracture Mechanics 27 (6), 615–642.

Ogden, R.W., 1984. In: Horwood, E. (Ed.), Non-linear elastic deformations. Halsted Press, New York.

Qu, J., Bassani, J.L., 1989. Cracks on bimaterial and bicrystal interfaces. Journal of the Mechanics and Physics of Solids 37 (4), 417–433.

Shivakumar, K., Chen, H., Smith S., 2003. An evaluation of data reduction methods for opening mode fracture toughness of sandwich plates, in: Proceedings of the 6th International Conference on Sandwich Structures, pp. 770–783.

Sun, C.T., Wu, C.L., 1991. Low velocity impact of composite sandwich panels, in: Proceedings of 32nd AIAA/ASME/ASCE Structures, Structural Dynamics and Materials Conference 1991, pp. 1123–1129.

Sun, C.T., Hasebe, R.S., 2000. Performance of sandwich structures with composite reinforced core. Journal of Sandwich Structures and Materials 2, 75–100.

Thomas, T., Mahfuz, H., Kanny, K., Jeelani, S., 2003. Dynamic compression of foam core sandwich composites, in: Proceedings of the 6th International Conference on Sandwich Structures, pp. 410–417.

Vadakke, V., Carlsson, L.A., 2003. Compression failure of glass/vinyl ester/PVC foam sandwich, in: Proceedings of the 6th International Conference on Sandwich Structures, pp. 127–141.

Veazie, D.R., Robinson, K.R., Shivakumar, K., 2003. Marine environmental effects on the interfacial fracture toughness of PVC core sandwich composites, in: Proceedings of the 6th International Conference on Sandwich Structures, pp. 485–495.

Wu, C.L., Weeks, C.A., Sun, C.T., 1995. Improving honeycomb-core sandwich structures for impact resistance. Journal of Advanced Materials (July), 41–47.

Zenkert, D., 1995. An Introduction to Sandwich Construction. Engineering Materials Advisory Services Ltd.